Energy and Displacement Demands Imposed on Rock Support by Strainburst Damage Mechanisms

P K Kaiser* and D A Malovichko**
*Laurentian University, Sudbury, Canada
** Institute for Mine Seismology (IMS), Hobart, Australia

ABSTRACT: Highly stressed excavations in hard brittle rock may fail by self-initiated, triggered or dynamically loaded strainbursts (Moss and Kaiser 2021). The low-frequency part of seismic radiation associated with strainbursts is described by a crush-type seismic source mechanism with a significant negative (implosive) isotropic component and a 'pancake-shape' CLVD deviatoric component. The seismic source is co-located with the excavation damage site. For such strainbursts, the ejection velocity is primarily related to the depth of strainbursting, the rock mass bulking characteristics, the duration of the bulking process, and the effectiveness of the support system. For dynamically loaded strainbursts, the displacement and energy demand may be augmented by the impact of the stress wave from a distant seismic event. This article describes the failure process and factors contributing to rock deformation and energy demands for support design. Case examples are used to demonstrate the dependence of rock displacements, rock ejection and energy demand on the factors described above. A seismic source model is proposed to assess the depth of strainbursting and the duration of the related bulking process by using seismic monitoring data. The implications for support design are briefly discussed.

INTRODUCTION

Mining companies working at great depth, typically exceeding 1500 m, have identified seismic hazards as a corporate risk and view ground control with reliable cost-effective support systems as a strategic tool in asset management. In highly stressed ground, the support must be designed for load equilibrium, displacement compatibility, and dissipation of kinetic energy imposed by a rockburst.

Historical developments

In the Canadian Rockburst Support Handbook (CRBSHB 1996; Chapter 6), the depth of failure for rockburst damage was estimated using a semi-empirical depth of failure chart. The deepening of the depth of failure was related to the stress wave intensity from a distant seismic event (i.e., to the peak ground motion (*PGV*)). The displacement imposed on the support was estimated using empirically established linear bulking factors (*BF*) ranging from *BF* = 10±3%, to 5±1% to 1.5±0.5% for light to yielding to strong support, respectively. A refined bulking factor graph was introduced by Kaiser (2016) highlighting the dependence of bulking on the imposed tangential straining at the strainburst location. In retrospect, the need to anticipate the ejection velocities for kinetic energy estimation, related to the observed distances of rock ejection (or to the ground motion from a distant seismic event), proved to be the weakest step in this design approach.

Since then, Heal et al. (2006) established that excavation damage should also depend on the vulnerability of the excavation. Morissette et al. (2012) demonstrated and confirmed that strainburst damage mechanisms dominate for seismic events with magnitudes *M* less than approximately two.

Diederichs (2018) recognized that structural controls strongly influence the depth of failure and the stress-induced rupture behaviour and offered a chart to estimate the energy demand as a function of the average failure thickness and ejection velocity (resulting in kinetic energy demands ranging from 0 to 60 kJ/m^2). The weak step in this approach remains as the ejection velocity must be known for kinetic energy calculation. The impact of distant seismic events is not considered and thus the approach is not applicable for dynamically loaded strainbursts.

Largely based on laboratory tests, Villaescusa et al. (2016, and in other related publications) introduced a chart relating the kinetic energy demand for support design to the thickness of the anticipated unstable mass and the *UCS* of the host rock. On this chart, the influence of geological structures on the depth of failure is recognized, however the impact of distant seismic events is no longer considered. In this

approach, the ejection velocity and thus the kinetic energy demand is directly related to the *UCS* with the ejection velocity ranging from 5 to 9.5 m/s for *UCS* = 75 to 225 MPa, respectively (also resulting in a kinetic energy ranging from 0 to 60 kJ/m^2). The weakness of this approach is that the ejection velocity is related to a single, highly variable parameter, i.e., the intact strength (*UCS*), without consideration of the loading system stiffness. The impact of the local mine system stiffness or the deformation potential on the unsupported ejection velocity is illustrated by Figure 1 for five post-peak stiffnesses (*k*). Accordingly, velocities exceeding 4 m/s are only to be expected in very to extremely soft loading systems, e.g., in wide excavations, at high excavation ratios, with dominant geological structures, and with an ineffective support. In these situations, the rock mass characteristics rather than the intact strength controls the energy release. In the authors' opinion, ejection velocities exceeding 4 to 5 m/s while physically possible due to magnification by momentum transfer, are rare and lead to unreasonably high energy demands (e.g., 5-times higher energy demand for 9 m/s than for 4 m/s).

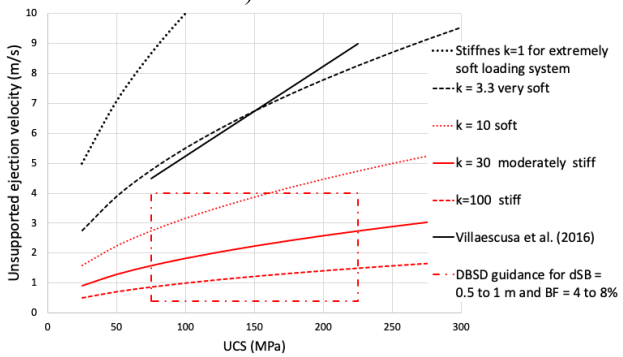

Figure 1 Unsupported rock ejection velocities for uniaxial loading of brittle failing rock (d_{SB} = depth of strainbursting; BF = linear bulking factor).

A further fundamental flaw of these energy-centric design approaches is that the energy demand is compared to the installed (undeformed) support capacity. Support capacity consumption is ignored. In mining, some of the support's capacity is consumed by static support deformation before rockburst loading and by dynamic deformation during the rockburst. For example, more support capacity is consumed near an undercut in highly stressed ground than in virgin ground without cave influence. As a dynamic energy demand is imposed on the support, the support is further deformed, and more capacity is consumed during the rockburst process. Therefore, the remnant energy capacity of the support after a rockburst is significantly lower than the installed capacity. This is schematically illustrated by Figure 2. Failure occurs when the dynamic demand (D), represented by the blue demand path, reaches the remnant capacity (C^r) shown in red. The installed energy capacity at zero displacement can never be reached during a rockburst.

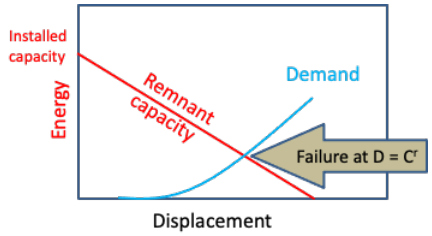

Figure 2 Schematic displacement vs support capacity chart with support failure when the displacement and energy demand (blue) reach the remnant support capacity (red).

Recent developments

Kaiser and Moss (2021) present a deformation-based support design (DBSD) approach for brittle failing ground to overcome these deficiencies and to account for the fact that displacements induced by mining or sudden stress-fracturing consume much of the support's installed capacity. They demonstrate that it is necessary to design the support for the remnant support capacity, i.e., the displacement and energy capacities remaining when the support is needed during and after a strainburst. For a rational support design, it is necessary to establish the demand path in the displacement – energy space (Figure 2). Means to estimate this demand path from seismic data are presented in this article.

Figure 3.a presents an illustrative example in the displacement – energy space for a single component support system consisting of a single bolt type (threadbar at 1x1 m spacing) and a robust areal support that is installed 25 mm before the bolts are activated. The remnant energy capacity (red) decreases as the support is deformed until it is fully consumed at 75 mm displacement (i.e., for an assumed work split factor m = 50% for equal allocation to direct straining at the plate and indirect straining of the threadbar inside the rock mass). The blue demand path describes the displacement and energy demand for a strainburst with an incremental depth of failure of 0.75 m (called depth of strainbursting rock d_{SB}), a bulking factor BF = 5%, and a bulking duration of t_R = 25 ms without simultaneous loading by a distant seismic event (PGV = 0 m/s). For this example, the deterministic demand slightly exceeds the remnant support capacity of 2.8 kJ/m^2 at 68 mm (Figure 3.a).

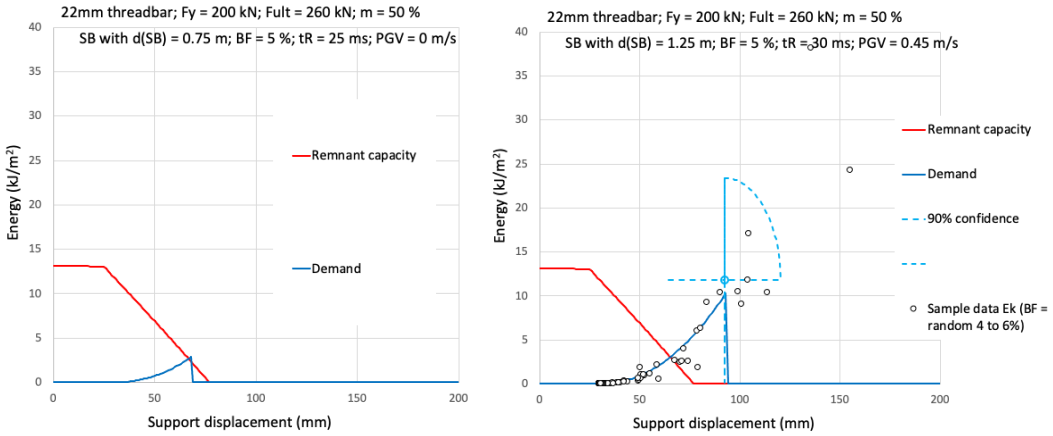

(a) (b)

Figure 3 Illustrative example of (a) remnant support capacity (red) and demand path (blue) for parameters listed in text, and (b) with 175 examples of displacement and energy demands estimated with the source model presented next for crush-type events.

Figure 3.b presents the estimated demand path (blue) for a more severe strainburst with d_{SB} = 1.25 m, a bulking factor BF = 5±1%, a slightly longer bulking duration of 30 ms, and with simultaneous loading by a distant event causing a ground motion PGV = 0.45 m/s at the strainburst location. As expected, the demand path exceeds the remnant capacity of a standard threadbar support system. The 90% confidence for a selected variability in design parameters (CoV ranging from 10 to 25 %) is indicated by the dashed displacement and energy ranges and by the quarter ellipse. For the simulated variability, the estimated displacement demand ranges from 65 to 120 mm and the energy demand from 0 to 23 kJ/m^2.

An example data set, obtained from 175 crush-type events following the procedure outlined next, are also presented in Figure 3.b. They follow the estimated demand path for d_{SB} = 1.25 m and all but one fall within the estimated confidence zone. Six exceed the deterministic demand, and one 'outlier' falls outside the 90% confidence limit suggesting a larger depth of strainbursting, more bulking and shorter bulking durations at the respective locations. For this data set, the crush-type events produce a displacement demand up to (160 mm - 30 mm =) 130 mm and an energy demand of up to 24 kJ/m^2.

This example demonstrates why a displacement – energy demand path is required for support design in burst-prone ground. Detailed explanations of the underlying deformation-based design principles are presented by Kaiser and Moss (2021). This article focuses on the use of seismic data to obtain the demand path for self-initiated and triggered strainbursts.

SEISMIC SOURCE MODEL

Two design parameters required for demand estimation can be estimated from seismic monitoring data: the depth of strainbursting d_{SB} and the bulking duration t_R. Seismic radiation associated with the dynamic fracturing of the rock mass surrounding a statically loaded tunnel by compressional stress was discussed by Malovichko and Rigby (2021) using the model reproduced in Figure 4. They show that the seismic radiation with wavelengths larger than the diameter of the tunnel and the extent of damage along its length (measured by L_3) is controlled by the elastic convergence of the surrounding rock mass rather than by rock fracturing. The source mechanism describing the low frequency (long wavelength) part of the seismic

radiation has a significant (more than 50%) implosive component and a negative (pancake-shape) Compensated Linear Vector Dipole (CLVD) component. The P-axis of the mechanism is approximately aligned with the direction of maximum compressional principal stress orthogonal to the tunnel's axis.

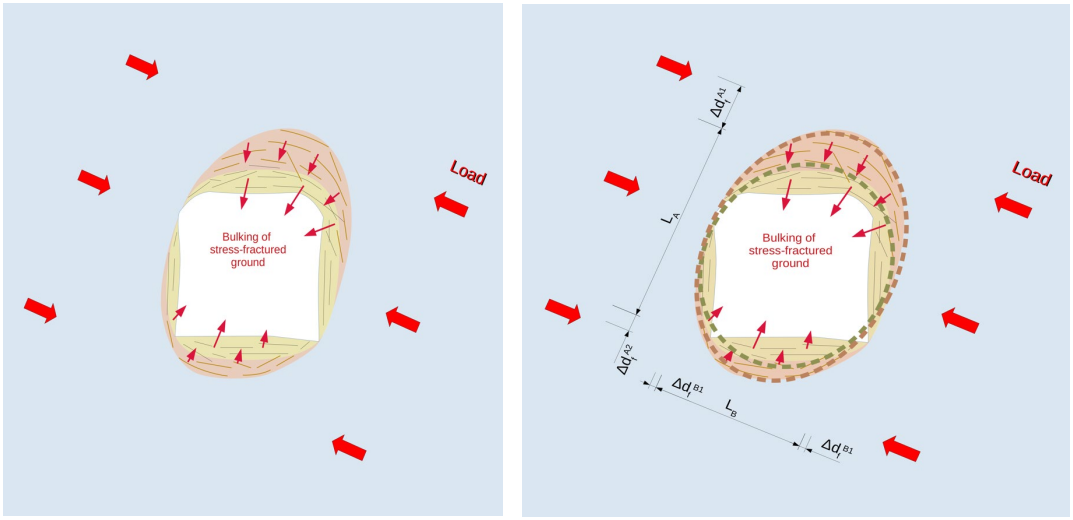

(a) (b)

Figure 4 (a) Conceptual model of fracturing around a tunnel; (b) approximation of a tunnel and its damage zone by pre- and post-strainburst elliptical cavities (Malovichko and Rigby (2021)). Δd_f corresponds to the depth of strainbursting d_{SB}.

It is assumed that the growth of the damage zone from brown to pink happens suddenly within a fraction of a second. The geometrical parameters of the model are shown in Figure 4 and are used to describe the seismic source mechanism. The scalar seismic moment[1] M_o can be approximated as:

$$M_0 = 2[(1-\nu)/(1-2\nu)]\,\sigma_{max}\,L_3\,D_A\,\Delta d_f^A\,, \qquad (1)$$

where ν is the rock mass's Poisson's ratio, σ_{max} the magnitude of the maximum principal stress orthogonal to the tunnel's axis, L_3 the length of dynamic fracturing along the tunnel, $d_{SB} = \Delta d_f^A = \Delta d_f^{A1} + \Delta d_f^{A2}$ the increase in depth of failure on both sides of the tunnel (orthogonal to σ_{max} and the tunnel's axis)[2], and $D_A = L_A + \Delta d_f^A/2$ the effective tunnel dimension (accounting for the pre-existing depth of failure $2(a + d_f)$ and half of increase in the depth of failure $\Delta d_f^A/2$).

The depth of bursting and associated convergence of the surrounding rock mass does not happen simultaneously and uniformly over the length of tunnel. It is reasonable to assume that the rupture process nucleates at some location, then evolves in space and finally ceases. These phases happen in a highly dynamic manner and radiate detectable seismic waves. The spatio-temporal evolution of the process can be described by decomposing it into a number of localized increments in the depth of failure $d_{SB}(X,t)$, where the coordinate X represents the location along the tunnel and t stands for time. The total duration of the process is called the bulking duration t_R. It can be assumed that the tunnel is straight and that elastic rock mass properties (e.g., ν), stress field (including σ_{max}) and geometrical characteristics of the tunnel (shape, effective dimension L_A) do not change along its length (i.e., along X). Therefore, seismic radiation from the localised increments in the depth of failure $d_{SB}(X,t)$ can be described by the same source mechanism (crush-type with constant orientation of P-axis) and the scalar moment presented in Equation (1) with all parameters fixed except of $\Delta d_f^A = d_{SB}(X,t)$. The kinematic model to arrive at $d_{SB}(X,t)$ is described in detail by Malovichko (2022). He also explains the assessment of parameters for this model (including $d_{SB(max)}$ and t_R) from the waveforms of seismic events.

---

[1] The scalar seismic moment adopted here is defined from seismic moment tensor as suggested by Silver and Jordan (1982): $M_o = sqrt(\Sigma M_{ij}^2/2)$. Note that there are alternative definitions, that produce different values of M_o for the same moment tensor (Bowers and Hudson, 1999).

[2] Note that the provided expression for M_o remains valid if the increase in the depth of failure only occurs on one side of the tunnel (i.e., Δd_f^{A1} or Δd_f^{A2} in Figure 4 can be zero). To simplify the notations, Δd_f will be used instead of Δd_f^A hereafter.

It is assumed that the bulking nucleates at location $X = 0$ and propagates symmetrically in both directions until it reaches $X = L_3/2$ and $X = -L_3/2$, and that the final profile of bulking $d_{SB}(X)$ for $-L_3/2 < X < L_3/2$ is parabolic and L_3 is constrained. $L_3 = n\, d_{SB}$ with n is set to 10 to 15 results in an intuitively acceptable range of L_3 of 5 to 30 m for $d_{SB} = 0.5$ to 2 m. Accordingly, as illustrated by the following figure, the highest E_{max} is encountered in the centre of L_3 and the average kinetic $E_{average}$ over the length of the burst is 46% for zero burden.

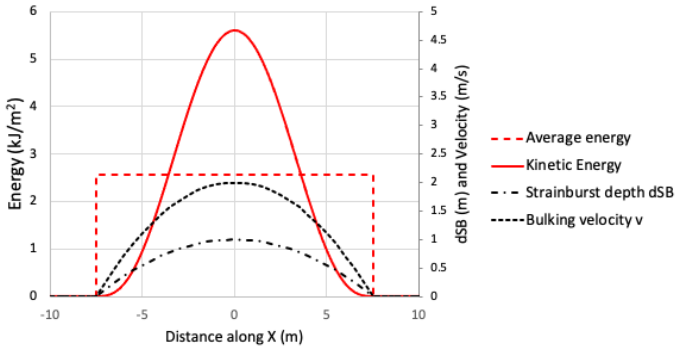

Figure 5 Energy release model along tunnel with E_{max} at centre and $E_{average} = 0.46\ E_{max}$; shown are depth of strainburst ($d_{SB(max)} = 1$ m) and bulking velocity at $BF = 5\%$ = constant for $t_R = 25$ ms.

ANALYSIS OF SEISMIC DATA

Before processing data for strainburst interpretation, it is important to identify (filter) relevant seismic events that apply the source model described in the previous section. The following data preparation procedure is suggested (and is adopted for this article):

- Select events with crush-type mechanisms according to classification shown in Figure 6.
- Some crush-type events may be associated with stopes or caves. These need to be excluded from the analysis as Equation (1) is not suitable for noncylindrical excavation shapes. Therefore, it is desirable to apply spatial filter covering individual tunnels.
- Small-size crush-type events may be related to the face of a tunnel and Equation (1) is again not applicable. Nevertheless, some crush-type events may correspond to stress-fracturing on the sides of the unsupported part of the tunnel in the proximity of its face. Although the Equation (1) may be legitimate for these events, their utility can be limited as the inferred parameters (d_{SB}, t_R) will not characterise the behaviour of supported ground. For this reason, it is preferable to select crush-type events around existing tunnels away from the advancing faces.

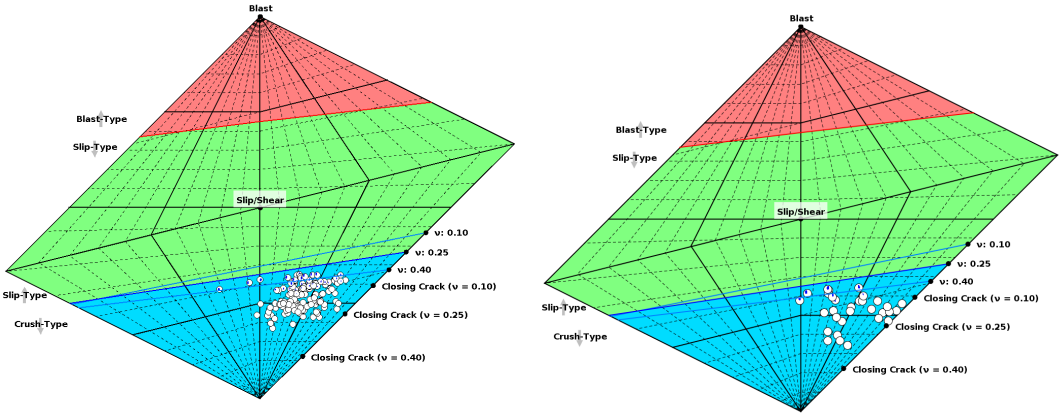

Figure 6 Source-type plot of Hudson et al. (1989) with classification zones suggested by Malovichko and Rigby (2021) and data set for Cases A and B. The boundaries between the classification zones are defined in terms of proximity to ideal mechanisms, which are as follows: Explosion (expansion of spherical cavity) for blast-type, Double Couple for slip-type and Closing Crack for crush-type. The location of ideal crush-type mechanism and boundary between slip-and crush-type zones depend on Poisson's ratio *v*.

ESTIMATION OF DEMAND PATH FOR STRAINBURSTS

Strainburst risk and failure process

As described by Moss and Kaiser (2021), there are three types of strainbursts:

- *self-initiated*, whereby the local mining-induced stress exceeds the rock mass strength and the rock 'explodes' without external energy input from a distant seismic source,
- *triggered*, whereby a distant seismic event triggers the failure process and the rock 'explodes' without significant energy input from the triggering seismic source, and
- *dynamically loaded*, whereby the stress-wave from a distant seismic event or from rupture along an excavation-scale geological structure contribute to the strainburst damage process by increasing the depth of failure, the bulking deformation, the bulking velocity; therefore, adding kinetic energy.

The first two strainburst types are recorded as crush-type seismic events and are the focus of this article. However, slip-crush-type events with an added displacement and energy component due to a locally elevated deformation potential can be treated in a similar manner for support design. Furthermore, even damage caused by a strong distant fault-slip event may include a strainburst component. In a slip scenario, a critically stressed excavation may also release energy close to the excavation by a sudden displacement imposed on the support due to bulking of stress-fractured rock.

The cause and effect of the strainburst process is presented in Figure 7.a. Local stress raisers (red areas in σ_1 contours) inside the rock mass surrounding an excavation (with or without weaknesses or joints) indicate locations of strainburst risk (yellow stars). Hard brittle rock, driven by the tangential stresses (brown arrows) or shear stresses on weaknesses, may 'explode' and bulk as illustrated by the photo overlay. As a result, broken rock is forced into the excavation and the average velocity of movement (displacement rate) is a function of the bulking volume, its bulking factor (BF) and the bulking duration (t_R). This velocity v_i impacts the burden of stress-fractured rock between the burst volume and the excavation wall (Figure 7.b) providing the burden and the burst volume or part of it with kinetic energy.

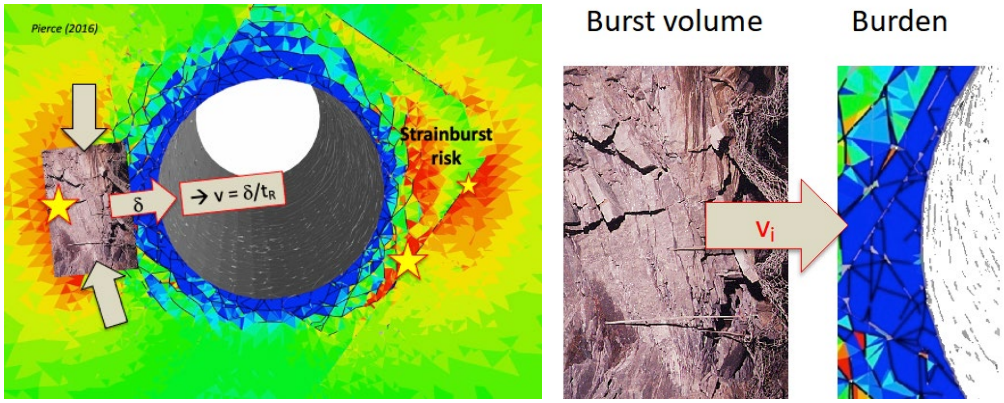

(a) (b)

Figure 7 (a) Stress conditions contributing the strainburst failure and the displacement rate v_i generated by bulking on the inside of the burst volume, and (b) velocity v_i impacting the burden of previously stress-fractured rock (Pierce (2016); pers. com.).

Estimation of displacement demand from strainbursts

At the excavation wall, the pre-burst displacement of the stress-fractured rock is given by $\delta_{ws} = d_f \cdot BF_{static.}$ This volume with a depth of statically fractured ground d_f constitutes the 'burden' that may be ejected by a deeper-seated strainburst. If rock support is installed before stress-fracturing, this displacement is imposed on the areal support and to a lesser extent to the bolt plates. It may consume part of the installed support capacity. This depth of failure can be obtained from probe hole drilling or observations during rehabilitation. For situations where data is lacking, the extreme depth of failure by spalling can be obtained from empirical relations; for example, from $d_f/a = (1.37\ SL - 0.51)$ (Kaiser (2016) with a = equivalent excavation radius, the calibrated $SL = \sigma_{max}/UCS$, the average depth of failure in a notch is approximately

2/3 d_f). If local, excavation-scale weaknesses in the rock mass are involved (e.g., persistent jointing as shown in Figure 7.a) or in blocky ground with block sizes less than approximately 1/10th of the excavation span, it is reasonable to assume a 45°-wedge/notch shape for a maximum $d_f = w/2$ or $h/2$ or an average of $d_{f(average)} = w/4$ or $h/4$.

At the inner boundary of the burst volume, the displacement imposed on the burden is $\delta_i = d_{SB} \cdot BF_{dynamic}$ causing a total wall displacement of $\delta_{wd} = \delta_i + \delta_{ws}$. The applicable depths of failure d_f, depth of bursting d_{SB} and bulking factors are obtained from field measurements or from empirical relations (Kaiser 2016). Most importantly, the d_{SB} can also be estimated from the seismic source model introduced earlier. The average bulking factor is obtained by measuring the depth of failure or bursting and the associated wall movement.

For situations where no site-specific data is available, e.g., during pre-feasibility studies, the following parameters can be used to arrive at initial displacement estimates:

- The depth of burden d_B = 0.3 to 0.5 m ($w/4$ or $h/4$ in blocky ground or with prevailing geological structures) for moderate to high stress levels SL.
- For standard drift sizes: d_{SB} = 0.5 m at moderate $SL < 0.8$ and 1 m at high $SL > 0.8$ ($SL = \sigma_{max} / UCS$; if SL is not calibrated use upper 75th percentile of UCS data; $\sigma_{max} = 3\ \sigma_1 - \sigma_3$).
- BF = 2 to 3% during mine development with light rock support and 4 to 8% at highly stressed or strained mining fronts (BF = 4 to 6% with effective support; BF >10% for unsupported floors).
- The resulting displacement demand at the excavation wall for the above listed data ranges from δ_w = 20 to 120 mm. It may be larger when local geological weaknesses magnify the deformation potential.

These parameters are based on field observations and back-analyses from various burstprone mines and should be verified by field observations upon access to stress-damaged ground.

Estimation of ground velocities from strainbursts

The average 'ejection' velocity or bulking velocity at the inner boundary of the burst volume is given by $v_i = d_{SB} \cdot BF_{dynamic}/t_R$. The bulking duration t_R can be estimated from distances of unsupported rock ejection or the seismic source model introduced earlier. The dynamic average bulking factor is obtained by measuring the depth of busting and the associated wall movement. Due to a lack of data, it is currently prudent to assume that $BF_{dynamic} \geq BF_{static}$.

For situations where no site-specific data is available, the following parameters can be used to arrive at initial velocity estimates: event duration t_R = 20 to 50 ms for d_{SB} = 0.5 to 1 m, resulting in a displacement rate v_i = 0.4 to 4 m/s for BF = 4 to 8%. It may be higher when local geological weaknesses magnify the deformation potential. These parameters are to be verified by field observations and seismic data analyses.

Estimation of kinetic energy demands from strainbursts

The kinetic energy demand from the bulking-induced displacement rate is $E_k = ½\ m\ v_i^2$. The mass m consists of the burden and part of the strainburst volume. In the extreme $m = (d_B + d_{SB}) \cdot \gamma$.

This energy estimate may be higher if excess stored strain energy (= stored strain energy – energy sinks such as friction, rupture energy, heat, …) is released or if energy is transferred to the ejectable mass from distant seismic sources.

For situations where no site-specific data are available, e.g., during pre-feasibility studies, the following kinetic energy demands from bulking during a strainburst can be anticipated assuming that half of the burst volume moves at v_i: For v_i = 0.4 to 4 m/s and $d_B + ½\ d_{SB}$ = 0.55 to 1 m with γ = 2,750 kg/m^3, E_k = 0.12 to 22 kJ/m^2. These parameters are to be verified by field observations and seismic data analyses.

Displacement - energy demand paths from strainbursts

Following the above-described approach and approximations, exemplary demand paths are presented in Figure 8 (for t_R = 20 to 32 ms; d_{SB} = 0 to 1.5 m; BF = 2, 4, 6 and 8%; no burden; and PGV = 0 m/s).

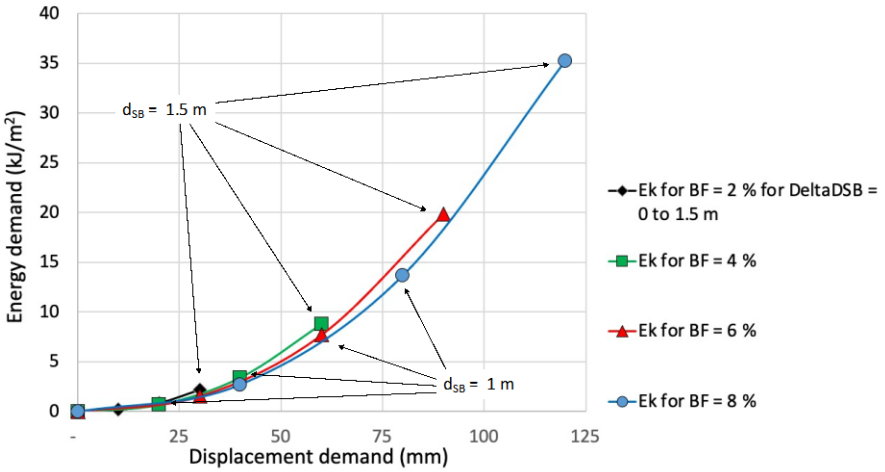

Figure 8 Demand paths for the preliminary support design when site-specific information is lacking: each path is for a constant bulking factor with strainburst depth of 0.5, 1 and 1.5 m.

The demand path is dominated by the bulking process: more bulking rock increases the displacement demand d, the initial velocity and thus the kinetic energy demand. For the chosen design parameters, the parabolic demand paths are approximately described by $E_k \propto d^{2.1}$ with the d_{SB} and BF determining the end point of the demand path. In other words, doubling the displacement demand approximately quadruples the energy demand. This figure illustrates a most important practical implication, i.e., the need for bulking controls to minimize support demand.

CASE STUDIES – DEMAND PATH ESTIMATION

Three case studies are presented next with information provided by mines with high quality data acquisition and processing capabilities. The process followed is:

- Determination of t_R, d_{SB} and selection of L_3 from seismic source model.
- Estimation of induced displacement for a designated bulking factor (for simplicity assumed to be constant at $BF = 5\%$ for the following illustration; a d_{SB}-dependent BF-rules could be applied). For this step, two solutions are presented: one-sided d_{SB} and two-sided with 50:50 split of d_{SB}. Practical experience shows that one-sided failures are more readily observed, except when floor heave or lower wall failures are involved.
- Estimation of bulking induced velocity at the inner boundary of the burst volume v_i. This velocity is double for one-sided bursting.
- Estimation of kinetic energy E_k (for simplicity, the burden is assumed to be constant at typically observed values of 0.3 or 0.5 m) for demand paths in the displacement – energy space. The energy release is more than quadruple for one-sided bursting due to the v_i^2-term in E_k calculation.
- Resulting endpoints of the demand paths are presented together in the displacement – energy graph.

Case A

This case of a narrow vein orebody with 123 crush-type events in an area with sub-horizontal P- axes suggests strainbursting in drift backs and floor bursting caused by high σ_1-values at the surface of these drifts (approximately 120 MPa from elastic model).

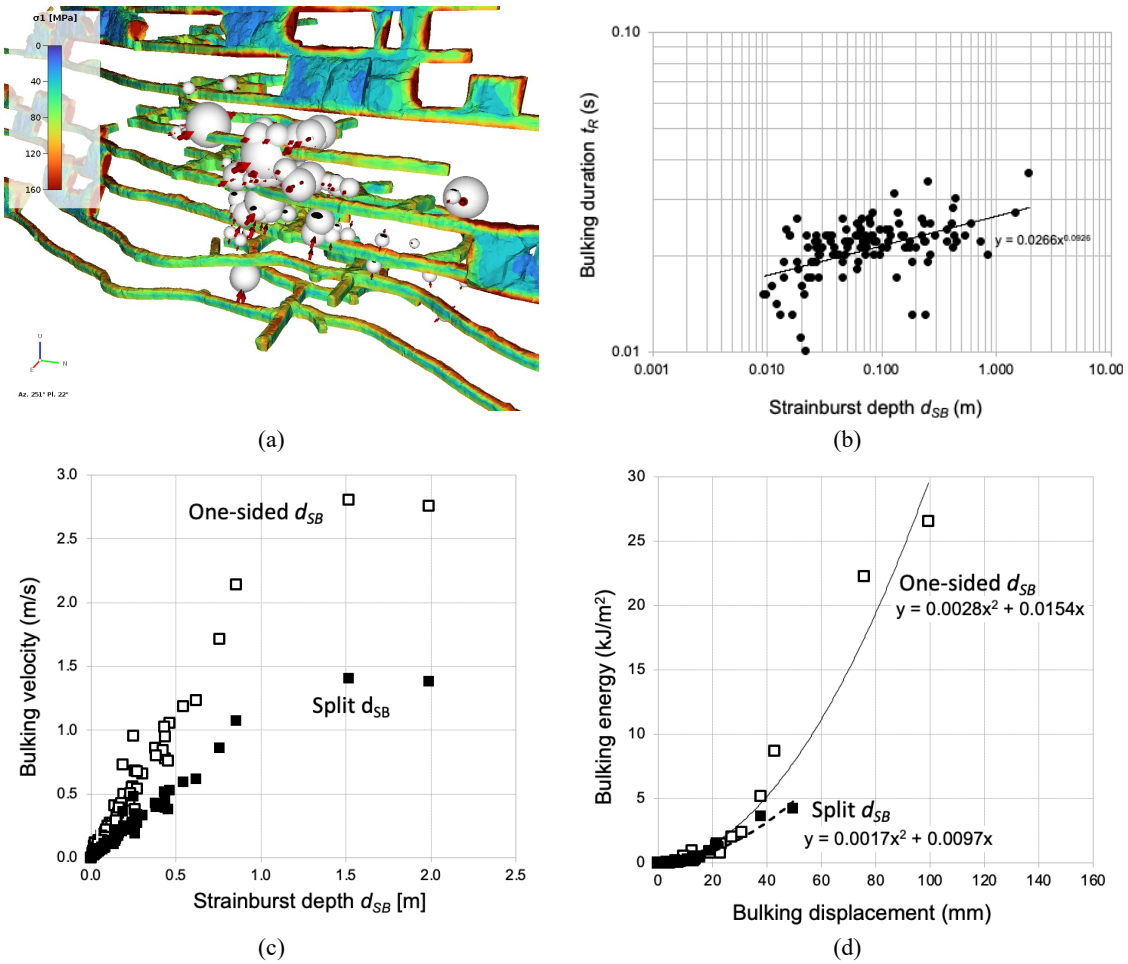

Figure 9 CASE A: Demand estimates using seismic source model: (a) Location of intense bursting with crush-type events and major principal stress contours; (b) depth of strainbursting d_{SB} vs bulking duration t_R; (c) d_{SB} vs bulking velocity v_i for one- and two-sided bursting at fixed rupture length ratio L_3/d_{SB} = 15; (d) end points of demand paths with polynomial trends for one-sided (empty squares) and two-sided (full squares) bursting.

The above figures are generated for the following common assumptions: constant burden of 0.5 m for high static stress level; constant bulking factor BF = 5%; no extraordinary influence of nearby geological structures; d_{SB} and t_R from source model with a constant L_3/d_{SB} = 15 with L_{3min} =3.5 m; strain energy in burst volume was consumed by supported rock mass; no dynamic loading from remote seismic events PGV = 0.

The bulking times range from 10 to 36 ms for the strainburst depth d_{SB} ranging from 0.01 to 2.0 m, respectively, resulting in one-sided bulking velocities up to 1.3 m/s for 97% of the strainbursts. Four events produce higher velocities up to 2.8 m/s. For both-sided bursting, the velocities were half (full squares).

With a non-bulking burden, the resulting displacement demands were ≤99 mm for one-sided and half for two-sided bursting. The maximum kinetic energy demand in the centre of L_3 was ≤10 kJ/m^2 for 98% of the strainbursts (with a stress-fractured rock burden of 0. 5 m).

Practical implication

For a given crush-type event intensity as recorded by seismic radiation, one-sided bursting causes higher displacement demands and bulking velocities (double) and consequently much higher energy demands (quadruple). Nonsymmetric failures are more violent and impose higher demand on the support.

Floor heave velocities may be higher than those shown in Figure 9.b as the bulking factor is likely 2 to 4 times higher in the unsupported floor. It is speculated that the larger events with d_{SB} = 1.5 to 3 m for one-sided bursting, involved floor heave. In that case, heave displacements of 75 to 300 mm with velocities of

1.5 to 6 m/s could be expected, leading to maximum free vertical throw heights between 0.1 and 1.8 m (1 m for 4.5 m/s).

The above quoted displacement and energy demands apply to the center of the cosine strainburst distribution shape along L_3. They are zero at $\pm L_3/2$. The average displacement is approximately 2/3 of the maximum bulking displacement and the average energy demand over L_3 approximately 46% of the maximum E_k due to the reduction in mass and velocity along L_3 (Figure 5). It is for this reason that localized support damage is often observed with decreasing deformation of the support away from the damage center.

Comparison of demand with a support capacity model (Kaiser and Moss, 2021)

The data is compared with the remnant capacity of a generic single component support system consisting of threadbar at 1x1 m spacing (Figure 3.a) and an estimated demand path for a self-initiated or triggered strainburst ($PGV = 0$) with $d_{SB} = 0.7$ and 1.0 m at $BF = 5\%$ and $t_R = 25$ ms (blue) in Figure 10. The 90% confidence limits of the demand are shown (dashed blue) for $CoV(d_{SB}, BF, t_R, d_B, PGV) = 10, 25, 20, 15, 0$ %, respectively. The support systems used by the mine differs from this generic support system used for illustrative purposes. Comparisons with observed excavation and support damage are not reported here.

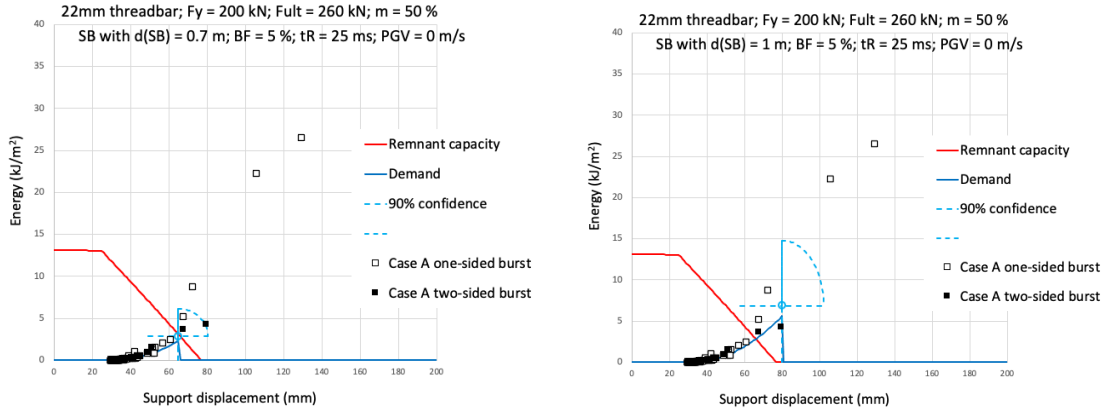

Figure 10 Illustrative example of remnant support capacity (red) for standard threadbar and demand path (blue) for parameters listed in text and figure titles, and with examples of displacement and energy demand estimates for Case A for crush events occurring after d_o = 30 mm of pre-event support deformation.

Figure 10 shows the individual strainburst demands (Figure 9.d) with an estimated demand path for a strainburst depth of 0.7 m (left) and 1 m (right) at $BF = 5\%$ (light blue). The demand path for $d_{SB} = 0.7$ m just reaches the remnant support capacity. All but three of the one-sided demands track the estimated demand path and fall within the 90% confidence limit. All two-sided demands fall inside the confidence limit. Only two of 123 or less than 2% of the recorded crush-type events exceed the demand estimated for a strainburst depth of 1 m.

The demand of 4 events or 3.3% exceed the remanent capacity of the standard threadbar support during one-sided bursting. The energy deficit (demand-remnant capacity) is huge for two one-sided events and severe excavation damage with rock and support ejection is expected for these events. For two two-sided events the energy deficit is much smaller and minor to moderate support damage is expected for these two events.

Case B

This mine is plagued by strainbursts and had to adjust mining to cope with stress-driven seismicity. 32 events were analyzed for one specific area in the mine. LiDAR measurements for the period which overlap with the seismic data indicated burst-induced movements (roof to floor) on the order of 0.1 to 0.2 m.

The following figures were generated for the following common assumptions: constant burden of 0.5 m for high static stress level; constant bulking factor $BF = 5\%$; no extraordinary influence of nearby geological structures; d_{SB} and t_R from source model with a constant $L_3/d_{SB} = 15$; strain energy in burst volume was consumed by supported rock mass; no dynamic loading from remote seismic events $PGV = 0$.

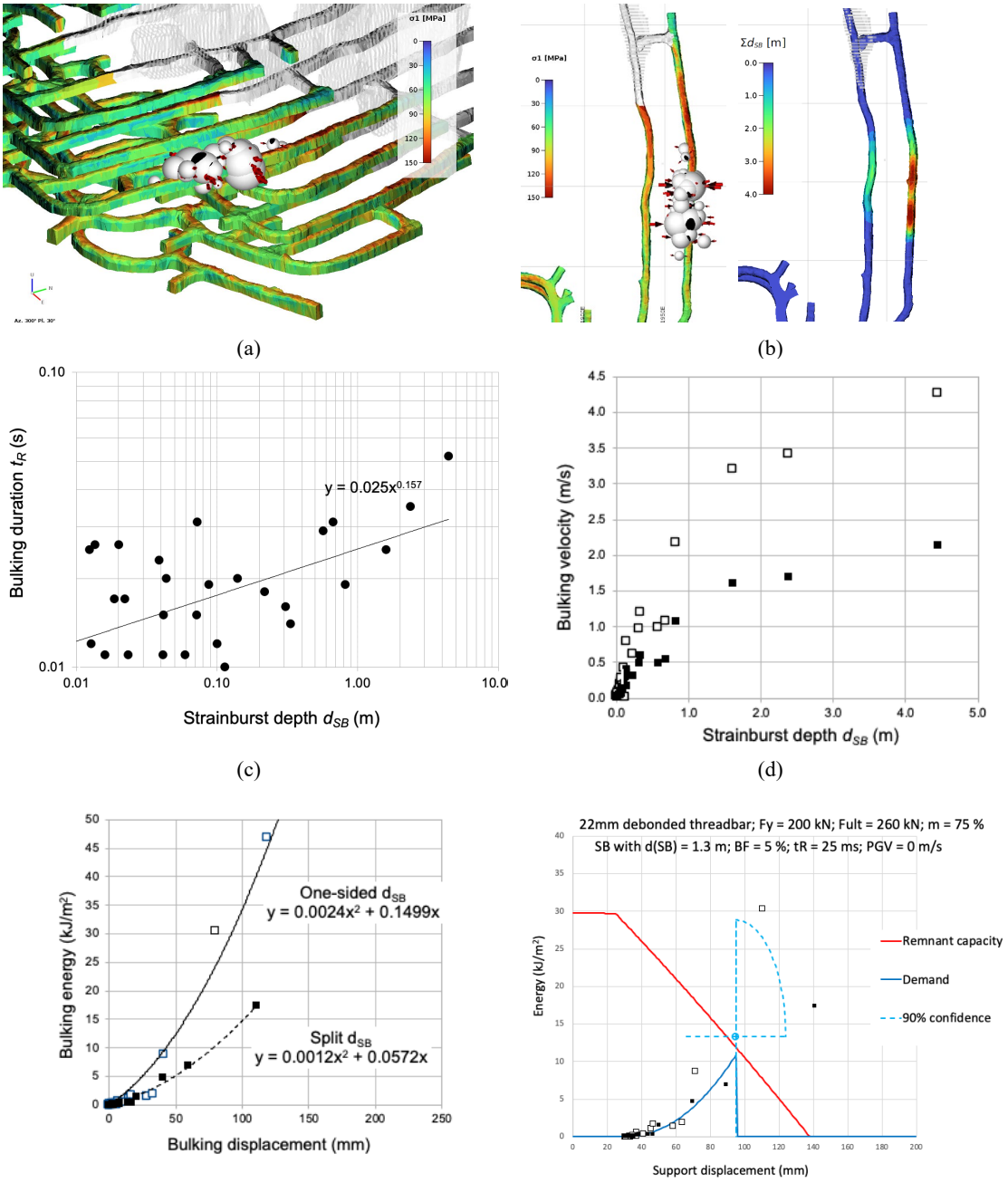

Figure 11 CASE B: Demand estimates using seismic source model: (a) Location of bursting with crush-type events and σ_1 contours; (b) plan views with σ_1 and with cumulative d_{SB} contours; (c) depth of strainbursting d_{SB} vs bulking duration t_R; (d) d_{SB} vs bulking velocity v_i for one-sided bursting at fixed rupture length ratio L_3/d_{SB} = 15 and L_{3min} = 3.5 m; (e) end points of demand paths with polynomial trend trends for one-sided bursting (one outlier is off-scale); (f) Illustrative example of remnant support capacity (red) for debonded threadbar and demand path (blue) for parameters listed in text. Also shown are displacement and energy demand estimates for one- and two-sided strainbursts.

The bulking duration ranged from 11 to 52 ms for the strainburst depth d_{SB} ranging up to 4.4 m, respectively, resulting in one-sided bulking velocities up to 1.1 m/s for 88% of the strainbursts. Four events produced higher velocities up to 4.3 m/s. For two-sided bursting, the velocities are half (full squares).

The cumulative depth of strainbursting is shown in Figure 11.b. The maximum LiDAR measurement for the burst period was ≤200 mm. With 0.5 m of non-bulking burden, the resulting displacement demands

were ≤119 mm for all but one at 240 mm one-sided (not shown) and half for two-sided bursting. The maximum kinetic energy demand in the centre of L_3 was ≤10 kJ/m^2 for 91% of the strainbursts. For 6% of the data, the kinetic energy demand exceeded 30 kJ/m^2 during one-sided bursting and 2% exceeded 20 kJ/m^2 for two-sided bursting.

The data are compared with an estimated demand path for d_{SB} = 1.3 m at BF = 5% and t_R = 25 ms (blue) in Figure 11.f. The 90% confidence limits of the demand are again shown (dashed blue) for CoV(d_{SB}, BF, t_R, d_B, PGV) = 10, 25, 20, 15, 0 %, respectively. They are also compared with the remnant capacity of a generic support system with debonded threadbar at 1x1 m spacing (again this is not the support used by the mine). This capacity was almost reached by the deterministic demand path (full blue curve) but was exceeded by the upper 90% confidence zone. All but one data point for one- and two-sided strainbursting fell within the confidence limits for the recorded crush-type events. Of these events 2 or 6.3% exceeded the remanent capacity of the debonded threadbar support during one- or two-sided bursting.

Case C

This sublevel caving mine does not experience strainburst problems. However, as the mine expands small crush-type events started to be observed in the deep part of the decline. This case is of interest as it illustrates the sensitivity of the demand estimation approach at early stages of strainbursting.

The following figures were generated for the following common assumptions: no burden for low static stress level; constant bulking factor BF = 5%; no extraordinary influence of nearby geological structures; d_{SB} and t_R from source model with a constant L_3/d_{SB} = 15; strain energy in burst volume was consumed by supported rock mass; no dynamic loading from remote seismic events PGV = 0. The source location accuracy was on the order of the drift scale.

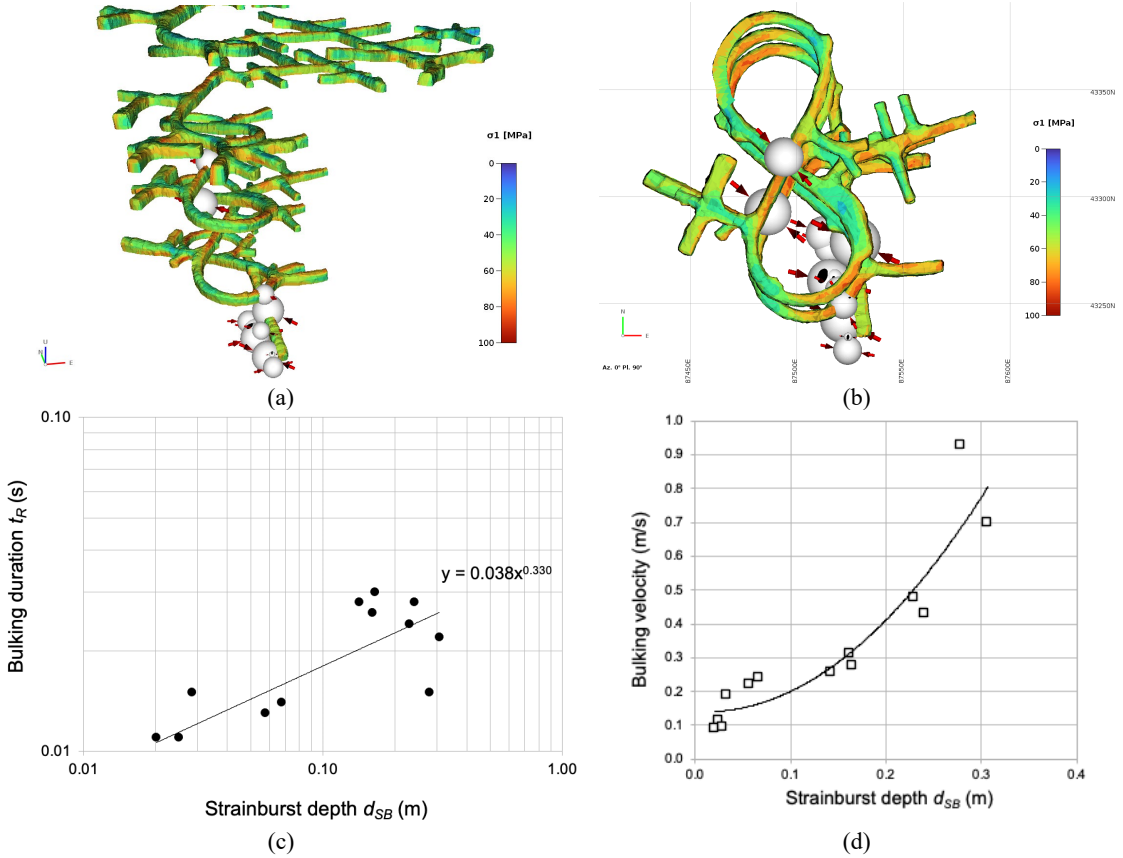

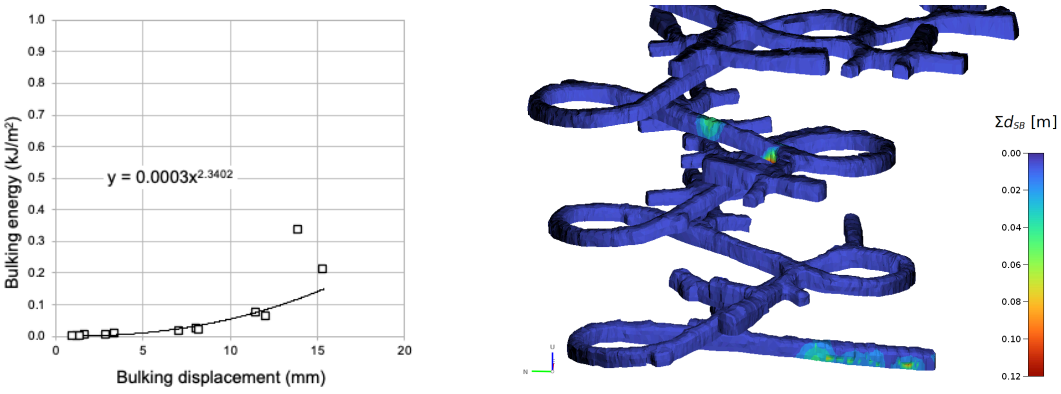

(e) (f)

Figure 12 CASE C: Demand estimates using seismic source model: (a) location of crush-type events and major principal stress contours from elastic model; (b) plan view; (c) depth of strainbursting d_{SB} vs bulking duration t_R; (d) d_{SB} vs bulking velocity v_i for one-sided bursting at fixed rupture length ratio $L_3/d_{SB} = 15$ for $L_3 > 3.5$ m; (e) end points of demand paths with polynomial trend trends for one-sided bursting; (f) Cumulative strainburst depth Σd_{SB}.

The bulking times range from 11 to 25 ms for the strainburst depth d_{SB} ranging from 0.02 to 0.31 m, respectively, resulting in one-sided bulking velocities up to 0.92 m/s. The resulting displacement demands were ≤16 mm for one-sided bursting and the maximum kinetic energy demand in the centre of L_3 is ≤0.34 kJ/m^2. This demand path will not cause support damage unless the support has been heavily pre-deformed. The cumulative depth of strainbursting (Figure 12.f) is currently localized and very small. Due to source location inaccuracy and the prevailing stress orientations (P-axes) strainbursting could be expected in the floor and/or roof.

These crush-type events of low intensity at this mine currently impose little displacement and energy demand on the support system. By monitoring future evolutions in the demand path, the mine will be able to establish rational support design criteria.

This case also serves to illustrate that the observation of crush-type seismic events does not necessarily imply significant excavations damage. If crush-type seismic events are small (in terms of seismic moment), then increase in the depth of failure d_{SB} and corresponding wall displacement δ_{wd}, may be minor and undetectable by visual inspections. However seismic data may still be useful, e.g., for the preliminary assessment of relation between d_{SB}, and t_R, or for the evaluation of expected bulking velocities v_i.

DISCUSSION AND CONCLUSIONS

Many mines around the world execute the following procedures to establish relations between observed rockburst damage and associated seismic source intensity: (a) measure distance R between the seismic source and location of damage, (b) evaluate the ground motion PGV at the location of damage using ground motion prediction equations (based on magnitude or other measures of source strength, e.g., seismic energy, moment or potency) and distance R to point source, (c) apply a seismic wave amplification factor, and (d) obtain an energy demand by squaring the ground motion and multiplying it by half of the ejectable mass.

As mentioned in this paper, PGV from a distant seismic event may be a relevant parameter for the assessment of energy demand in cases of dynamically loaded strainbursts. Although the procedure of PGV assessment may be applicable, the approach described above may result in misleading parameters:

– The location of seismic sources may be uncertain for several seismological reasons (e.g., errors in picking of P- and S-wave arrivals, inadequate velocity model). Seismic source locations, originally located more than 100 m from the place of damage, often are located much closer (within few tens of meters) to the damage after reprocessing. It is recommended to involve location uncertainty in the back-analysis of damaging seismic events and to always test the scenario of the seismic source being collocated with the damage (particularly for crush-type events).

– The source of significant seismic events may have a substantial spatial and temporal extent. For example, fault rupture may start at a specific location and propagate along a fault with time.

Therefore, the place of damage may be far from the location of source initiation (hypocentre), but close to the rupture surface. Conventional processing of seismic data is based on the initial arrivals of P- and S-waves and, therefore, provides the location of source initiation. It is recommended to use the distance to rupture plane instead of the hypocentral distance (distance to initiation) as R in ground motion prediction equations. This practice is adopted in earthquake engineering.

– The velocity of ground motion associated with seismic waves may be amplified significantly on the surface of excavations. However, this amplification can typically be attributed to high frequencies (e.g., above 100 Hz) and the resulting amplification of the ground motion displacement remains low. This may generate wave reflections leading to shotcrete rain, but the relative displacement of supported ground and host rock will not be 'amplified' and, consequently, ground support system loads may not or only marginally be affected by the wave amplification. It is recommended to be cautious with the application of an amplification factor to PGV without taking the frequency content of the ground motion and the resonance characteristics of the supported ground into account.

Conventional seismic source parameters inferred from waveforms of seismic events in mines are based on the assumption that the source represents an episode of shear rupture or fault slip in confined environments (double-couple source model for slip-type source). However, it is now recognized that seismic radiation for some events in mines cannot be explained by a double-couple source model and their interpretation in terms of shear failure or fault slip in a confined environment is not valid. These events must be interpreted in terms of sudden bulking of stress-fractured ground ('explosion' of the burst volume) near the perimeter of an excavation and associated convergence of the surrounding rock mass ('implosion' or crush-type sources). The source parameters derived assuming standard shear crack models are not legitimate for this failure process. This paper demonstrates the utility of an alternative source model that describes seismic radiation for sudden, violent bulking of stress-fractured ground on the perimeter of tunnels. Note that the parameters of this model (increase in the depth of failure, duration of convergence) make it possible to directly characterise the loading path of ground support by strainbursts without involvement of ground motion prediction equations.

For a support design it is demonstrated that the failing rock during strainbursts (crush-type events) imposes displacement and energy demands on the support. The methodology presented allows to estimate this demand path. For such strainbursts, the ejection velocity is primarily related to the depth of strainbursting, the rock mass bulking characteristics, the duration of the bulking process during the crush event, and the effectiveness of the support system. For self-initiated or triggered strainbursts, the ejection velocity is not related to the ground motion intensity from a distant seismic event. For dynamically loaded strainbursts, the displacement and energy demands may be augmented by the impact of the stress wave from a distant seismic event.

The case examples demonstrate the dependence of rock displacements, rock ejection, and energy demand on the contributing factors described above. The proposed seismic source model provides the depth of strainbursting and the duration of the related bulking process using seismic monitoring data recorded at mines. In this manner, it is possible to arrive at rational support designs for strainbursting ground. A most important practical conclusion is that one-sided bursting imposes much higher demands in terms of displacement (2-times higher) and energy (4 times higher) on the support than two-sided bursting. Consequently, if one side is effectively supported, the other side may experience more severe damage.

The ground support demand path assessment demonstrated in the paper is based on the analysis of seismic data and strainbursts which occurred in the past. As a mine evolves over time and stress conditions change it is important to forecast the values of strainburst depth and bulking duration that may be relevant in the future. The bulking duration may be inferred from the depth of bursting based on mine- or area-specific correlations, like the ones shown in Figure 9.b, 11.c and 12.c. The depth of strainbursting probably needs to be correlated with other parameters (e.g., rock mass properties, loading system stiffness, ground support characteristics). Back-analysis of observed crush-type seismic events should help to establish such correlations.

Another aspect for future work is related to the assessment of ground support capacity consumption. The regular measurements of surface displacement (e.g., LiDAR scans) offers an appropriate approach for it. However, only a few rockburst-prone mines acquire such measurements on a routine basis. This paper (maps of Σd_{SB} in Figure 11.b and 12.f) shows that seismic data can potentially be used to identify locations with support capacity consumption.

Ideally, it will be useful to have a probabilistic framework of strainburst damage assessment, which provides the maps of likelihood of damage for different parts of the mine and various time periods in the future. The demand-vs-capacity model discussed in the paper offers the core principles for a probabilistic framework. However, several components require further research (e.g., forecasting of d_{SB}).

ACKNOWLEDGEMENTS

The authors like to acknowledge Alex Rigby (IMS) for assisting with stress modelling for the case studies. The authors also wish to thank the companies that approved use of their data in an anonymous manner.

REFERENCES

Bowers, D. and J.A. Hudson (1999) Defining the scalar moment of a seismic source with a general moment tensor, Bulletin of Seismological Society of America, **89**(5), 1390-1394.

CRBSHB (1996) - Canadian Rockburst Support Handbook. https://www.geo-kaiser.ca/www.geo-kaiser.ca/wp-content/uploads/Publications/CRBSHB%201996%20Kaiser%20et%20al.pdf

Diederichs, M.S. (2016) Early assessment of dynamic rupture hazard for rockburst risk management in deep tunnel projects. J South African in Inst. of Mining and Metallurgy, 118: 193-204.

Heal, D., Potvin, Y. and M. Hudyma (2006) Evaluating rockburst damage potential in underground mining. ARMA/USRMS 06-1020, 12 p.

Hudson, J.A., Pearce, R.G. and R.M. Rogers (1989) Source type plot for inversion of the moment tensor, *Journal of Geophysical Research*, **94**(B1), 765–774.

Kaiser, P.K. and A. Moss (2021) Deformation-based support design for highly stressed ground with focus on rockburst damage mitigation. *J. Rock Mech. Rock Eng., open source available on-line, in press.*

Kaiser, P.K. (2016) Ground Support for Constructability of Deep Underground Excavations – Challenges of managing highly stressed ground in civil and mining projects. Sir Muir Wood lecture of International Tunnelling Association at World Tunnelling Congress, San Francisco, 33 p

Malovichko, D. and A. Rigby (2021) Description of seismic sources in underground mines: Dynamic stress fracturing around tunnels and strainbursting, Submitted to *Bulletin of Seismological Society of America*.

Malovichko, D. A. (2022) Utility of seismic source mechanisms in mining. Keynote paper at RASIM10.

Morissette, P., Hadjigeorgiou, J. and D. Thibodeau (2012) Validating a support performance database based on passive monitoring data. Deep mining, Perth 27-40.

Moss, A. and, P.K. Kaiser (2021) An operational perspective to ground control in deep mines. *J. Rock Mech. Rock Eng., open source available on-line, in press s.*

Silver, P.G. and T.H. Jordan (1982) Optimal estimation of scalar seismic moment, *Geophysical Journal of the Royal Astronomical Society*, **70**(3), 755–787.

Villaescusa, E., A. Kusui and C. Drover (2016) Ground support design for sudden and violent failures in hard rock tunnels. *Asia Rock Mechanics Symposium ARMS9,* 18 *p.*